electronics

MDPI

Article

Using Breast Tissue Information and Subject-Specific Finite-Element Models to Optimize Breast Compression Parameters for Digital Mammography

Tien-Yu Chang [1], Jay Wu [2,*], Pei-Yuan Liu [2], Yan-Lin Liu [2], Dmytro Luzhbin [3] and Hsien-Chou Lin [4]

[1] Department of Radiology, Cheng Hsin General Hospital, Taipei 112401, Taiwan; cty50961@gmail.com
[2] Department of Biomedical Imaging and Radiological Sciences, National Yang Ming Chiao Tung University, Taipei 112304, Taiwan; pattyliu820610@gmail.com (P.-Y.L.); akito0917@gmail.com (Y.-L.L.)
[3] Institute of Statistical Science, Academia Sinica, Taipei 115201, Taiwan; luzhbin@gmail.com
[4] Mechanical and System Engineering Program, Institute of Nuclear Energy Research, Atomic Energy Council, Taoyuan 325207, Taiwan; juy@iner.gov.tw
* Correspondence: jaywu@nycu.edu.tw; Tel.: +886-2-28267134

Abstract: Digital mammography has become a first-line diagnostic tool for clinical breast cancer screening due to its high sensitivity and specificity. Mammographic compression force is closely associated with image quality and patient comfort. Therefore, optimizing breast compression parameters is essential. Subjects were recruited for digital mammography and breast magnetic resonance imaging (MRI) within a month. Breast MRI images were used to calculate breast volume and volumetric breast density (VBD) and construct finite element models. Finite element analysis was performed to simulate breast compression. Simulated compressed breast thickness (CBT) was compared with clinical CBT and the relationships between compression force, CBT, breast volume, and VBD were established. Simulated CBT had a good linear correlation with the clinical CBT (R^2 = 0.9433) at the clinical compression force. At 10, 12, 14, and 16 daN, the mean simulated CBT of the breast models was 5.67, 5.13, 4.66, and 4.26 cm, respectively. Simulated CBT was positively correlated with breast volume ($r > 0.868$) and negatively correlated with VBD ($r < –0.338$). The results of this study provides a subject-specific and evidence-based suggestion of mammographic compression force for radiographers considering image quality and patient comfort.

Keywords: mammography; breast magnetic resonance imaging; compressed breast thickness; compression force

Citation: Chang, T.-Y.; Wu, J.; Liu, P.-Y.; Liu, Y.-L.; Luzhbin, D.; Lin, H.-C. Using Breast Tissue Information and Subject-Specific Finite-Element Models to Optimize Breast Compression Parameters for Digital Mammography. *Electronics* **2022**, *11*, 1784. https://doi.org/10.3390/electronics11111784

Academic Editor: Dong-Joo Kim

Received: 6 May 2022
Accepted: 2 June 2022
Published: 4 June 2022

1. Introduction

Digital mammography has high sensitivity and specificity for detecting microcalcification and mass in breasts [1]. It has become a front-line tool for clinical screening for breast cancer. However, the breast must be mechanically compressed during examinations. Insufficient compression force results in high compressed breast thickness (CBT), which reduces image quality and increases breast dose [2]. On the other hand, vigorous compression makes the patient uncomfortable during imaging procedures [3]. Some women even refuse mammography because of the painful experience. The compression force is closely related to breast volume and density [4]. Therefore, the use of breast tissue information may help us to determine objective recommendations for mammographic compression.

Asian women generally have denser mammary glandular tissue, and breast cancer occurs at a younger age compared with women in Europe and the United States. Breast ultrasound is often the first examination, especially for those who already have symptoms. However, breast ultrasound cannot detect microcalcifications in the case of carcinoma in situ. Digital mammography has thus become the primary method of screening asymptomatic and high-risk women. Breast tomosynthesis is a new technique that has been designed

to reduce tissue overlap for the extremely dense breast. It provides better visualization and characterization of tumor mass, asymmetric density, and architectural distortion in the breast, thus reducing the number of unnecessary biopsies. Breast magnetic resonance imaging (MRI) has increasingly been used for the diagnosis of mammographically occult cancer [5]. Breast MRI provides three-dimensional and multi-axis imaging with high tissue contrast, making it suitable for evaluating breast volume and density and constructing digital breast models.

To bridge the gap between breast MRI and mammography, simulation of breast compression using the finite element method (FEM) has been performed for breast tumor excision [6] and breast imaging [7]. Shih et al. [8] used MR images and the hyperelastic model to simulate four cases of breast compression in craniocaudal (CC) and mediolateral oblique (MLO) views. Thanoon et al. [9] applied the neo-Hookean model to simulate breast deformation after breast preservation therapy. Pianigiani et al. [10] inserted several nodules into the breast model to predict a large deformation of breast tissue. Lapuebla-Ferri et al. [11] produced virtual mammograms and tracked breast lesions across different views. Other studies have investigated the deformation and registration of breast lesions between different imaging modalities [12–14]. To our best knowledge, no studies have performed clinical validation of mammographic CBT for FEM simulation.

In clinical practice, the compression force applied for digital mammography is highly dependent on radiologic technologists [15]. Currently, there are no scientific recommendations regarding the appropriate compression force or CBT during mammography. The objective of this study was to establish the relationships between compression parameters of mammography and tissue parameters of breast MRI using FEM. Bridging the gap between these two modalities can provide evidence-based mammographic compression guidance under consideration of patient comfort, image quality, and radiation dose.

2. Materials and Methods

2.1. Case Collection

A total of 65 subjects were recruited for digital mammography and breast MRI within one month. The age of the subjects ranged from 45 to 69 years, with a mean age of 49 years. The inclusion criteria were women over 45 years of age and registered in the Taiwanese National Cancer Screening Program for breast cancer screening every two years. The exclusion criteria were women who had any of the following conditions: suspected or confirmed breast tumors, breast implants, and breast mastectomy. The research procedures were approved by the Institutional Review Board of Chi Mei Medical Center (No. 10002-012), and all subjects gave their written informed consent.

2.2. Image Acquisition

A Senographe DS system (GE Healthcare, Milwaukee, WI, USA) was used to perform digital mammography. The CC view was acquired with a compression force greater than 10 daN, which is recommended by the Taiwan Health Promotion Administration for full-field digital mammography. If subjects verbally expressed severe pain during breast compression, their image data were excluded from the analysis. The corresponding CBT was recorded and the breast imaging reporting and data system (BI-RADS) classification was performed according to the 5th edition of BI-RADS [16]. For breast MRI, an Aurora 1.5T dedicated breast MRI system (Aurora Imaging Technology, North Andover, MA, USA) was used to acquire T2 images with a flip angle of 45 degrees, a repetition time (TR) of 29 ms, an echo time (TE) of 4.8 ms, and a slice thickness of 1.125 mm. Each breast MRI dataset comprised 160 axial images, and each image had a matrix size of 512×512 and a pixel size of 0.7×0.7 mm^2.

In terms of image quality, mammograms should have uniform exposure, good image contrast, full tissue coverage, correct breast positioning, and no motion blurring, whereas breast MR images should not have motion artifacts, inhomogeneous fat saturation, phase wrap, and chemical shift. The acquired images were further verified for the above criteria

by a senior radiologist. Finally, a total of 40 breast datasets with both MR images and mammograms were used for modeling and compression simulation.

2.3. Image Segmentation

Three-dimensional breast models were constructed using MR images. A standard region growth algorithm was applied with a seed point manually placed in the breast to outline the contours of the breast. The chest wall and pectoralis major were excluded from the calculation of breast volume. Glandular tissue was then segmented using pixel values ranging from 900 to 1000 according to the histogram of MR images. The difference set between the entire breast and the glandular region was taken as adipose tissue. Volumetric breast density (VBD) was calculated as the ratio of glandular volume V_g to breast volume V_b. Figure 1 shows a computer-aided design (CAD) model with a breast volume of 286.8 cm^3 and a VBD of 18.9%.

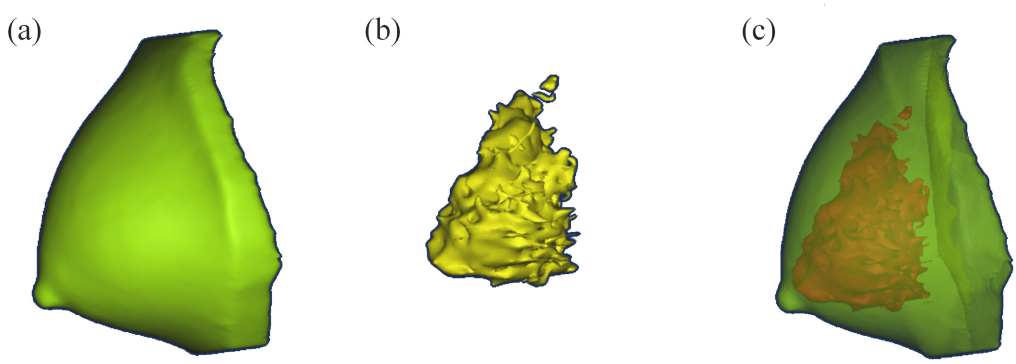

Figure 1. CAD model of a breast including (**a**) the contour of the breast, (**b**) the glandular tissue, and (**c**) the distribution of glandular tissue in the breast. Breast volume, glandular volume, and VBD are 286.8 cm^3, 54.0 cm^3, and 18.9%, respectively.

2.4. Finite Element Modeling

A two-dimensional (2D) mesh was built using a set of quads to define the outer surface of breast models. A tetrahedral volume mesh was then generated with an edge length of the element of 4 mm to compose the internal structure. On average, a total of 3270 nodes and 28,977 elements were required to compose a model. Abaqus (Dassault Systèmes, Waltham, MA, USA) was used to simulate compression of the breast model, where the Mooney-Rivlin biomechanical model was applied to address tissue behavior. The C_{10} and C_{01} material parameters of the biomechanical model were set as 2000 Pa and 1333 Pa, respectively, for adipose tissue and 3500 and 2333.3 Pa for glandular tissue [17].

The breast model was placed between a fixed support paddle and a compression paddle which exerted a downward movement during compression. The displacement of the nodes belonging to the chest wall and pectoralis muscle was set to zero as a boundary condition. During FEM simulation, the applied force and the corresponding paddle displacement were recorded. The distance between the two paddles is denoted as simulated CBT. The clinical CBT of the subject was compared with the simulated CBT at the clinical compression force of the subject. Furthermore, the breast model was compressed by 10, 12, 14, and 16 daN to investigate the simulated CBT as a function of breast volume and VBD.

3. Results

Figure 2 illustrates the distributions of clinical CBT obtained from digital mammography and breast volume and VBD obtained from breast MRI. The clinical CBT ranged from 2.3 to 8.1 cm with a mean value of 4.68 cm, which is similar to the average CBT of Taiwanese women [18]. The breast volume ranged from 232 to 1358 cm^3 with a mean value of 575.7 cm^3, and VBD ranged from 1.4% to 42.5% with a mean VBD of 16.0%. Figure 3a shows the correlation between breast volume and clinical CBT with a Pearson correlation coefficient r of 0.900 ($p < 0.001$), suggesting a significant positive correlation. Figure 3b

shows the correlation between VBD and clinical CBT. A moderately negative correlation ($r = -0.474$, $p < 0.05$) was observed.

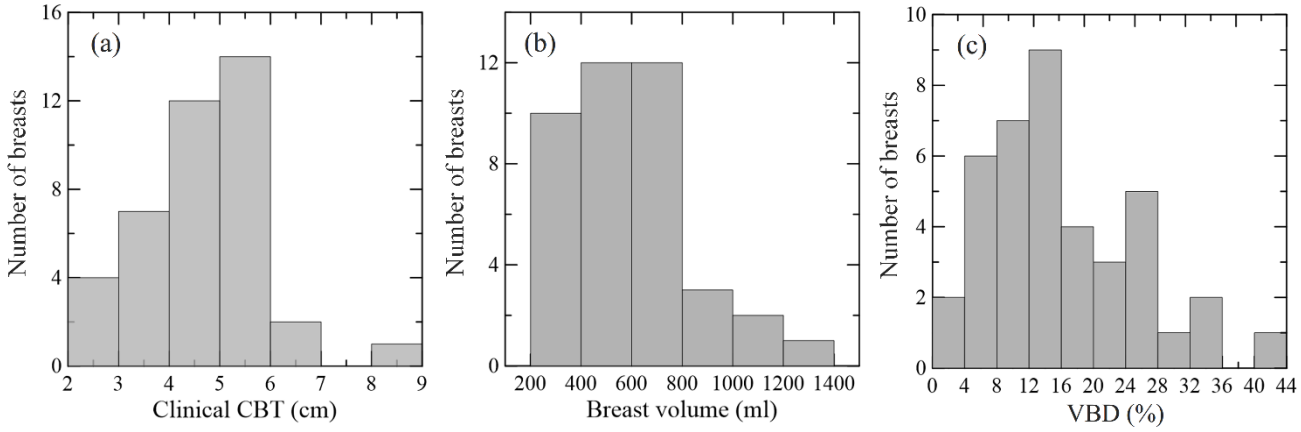

Figure 2. Distributions of (**a**) clinical CBT, (**b**) breast volume, and (**c**) VBD.

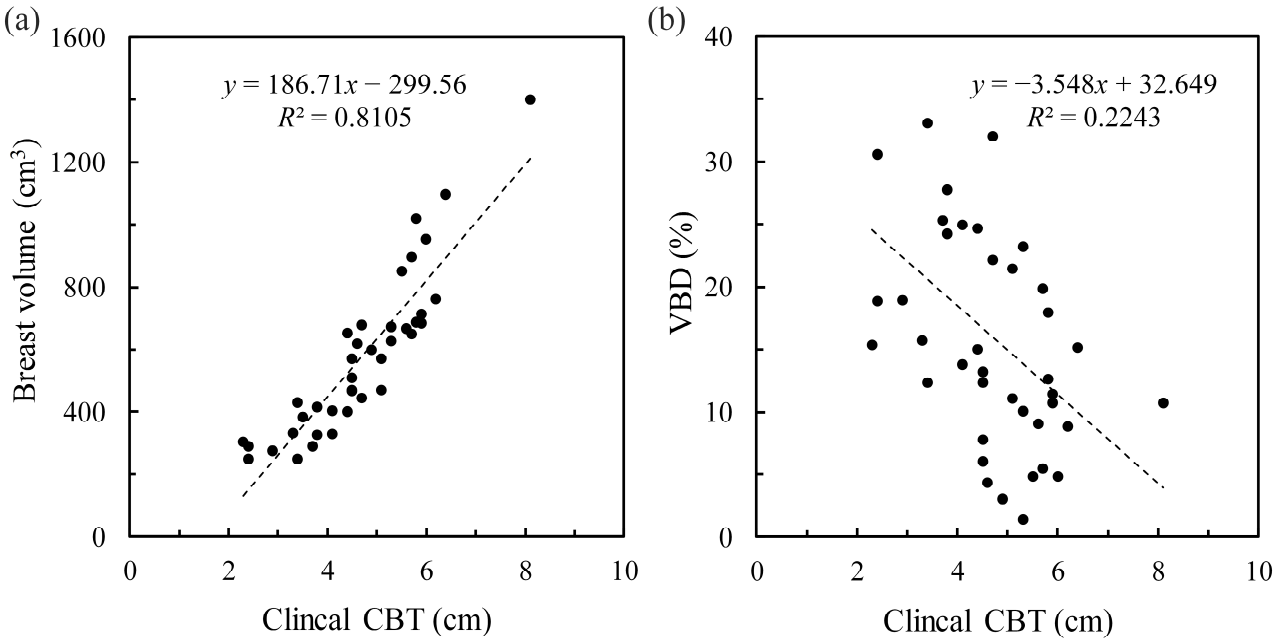

Figure 3. (**a**) Strong positive correlation between breast volume and clinical CBT ($r = 0.900$) and (**b**) moderately negative correlation between VBD and clinical CBT ($r = -0.474$).

The box plot of VBD obtained from breast MRI for different categories of BI-RADS obtained from mammography is shown in Figure 4. The most frequently occurred BI-RADS category was c, followed by d and b, and the corresponding mean VBD was 14.7, 19.7, and 3.6%. No cases of category a were recorded. Although the VBD and BI-RADS category exhibited a positive correlation, the widespread and overlapping distribution of VBD between each category infers that the BI-RADS classification is influenced by observers and cannot accurately quantify breast density.

Figure 5 shows the compression force as a function of paddle displacement for different volumes of breast models. The compression force increased dramatically when the displacement exceeded 60 mm. The breast volume did not significantly affect the shape of the curve. Figure 6 illustrates node displacement in the compressed breast model of the left breast of a 52-year-old woman, whose breast tissue parameters are $V_b = 670.3$ cm^3, $V_g = 155.6$ cm^3, and VBD = 23.2%. At the same compression force of 15 daN, the simulated CBT and the clinical CBT were 5.6 cm and 5.3 cm, respectively. The tissue in the outer

region of the breast model was moved outward and backward, whereas the tissue in the inner region was moved outward and forward.

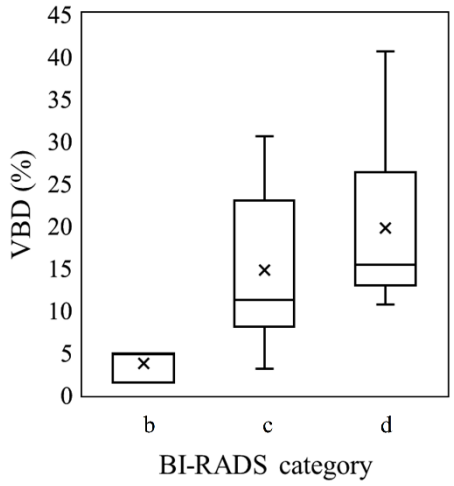

Figure 4. Box plot of VBD for b, c, and d BI-RADS categories. The horizontal line in the box represents the median, and the box contains the 25–75 percentiles. No cases of BI-RADS category a were recorded in this study.

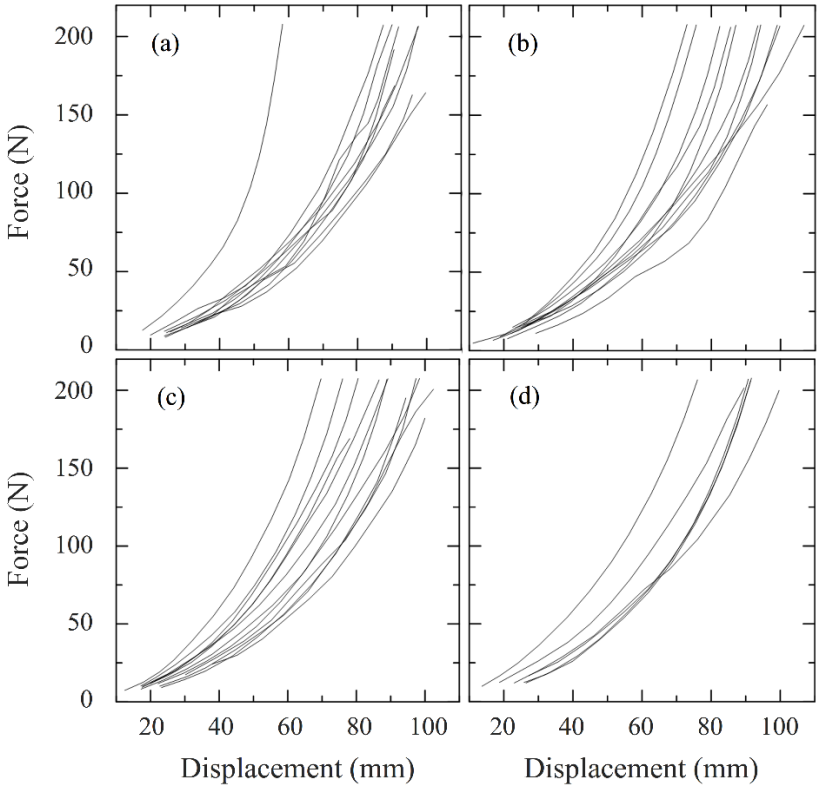

Figure 5. Applied force versus paddle displacement for breast models of (**a**) 200–400, (**b**) 400–600, (**c**) 600–800, and (**d**) 800–1400 mL.

Figure 7a shows the scatter plot of the simulated CBT obtained from the breast models and the clinical CBT obtained from mammography at the same clinical compression force. The simulated CBT increased as the clinical CBT increased with good fitting linearity (R^2 = 0.9433). The studentized residual as a function of clinical CBT is shown in Figure 7b. The residuals were randomly scattered without showing any noticeable trend. A paired sample *t*-test was performed at a 95% confidence level, showing no significant differences

(p = 0.564). These results demonstrate the accuracy of FEM and mechanical deformation of the breast models.

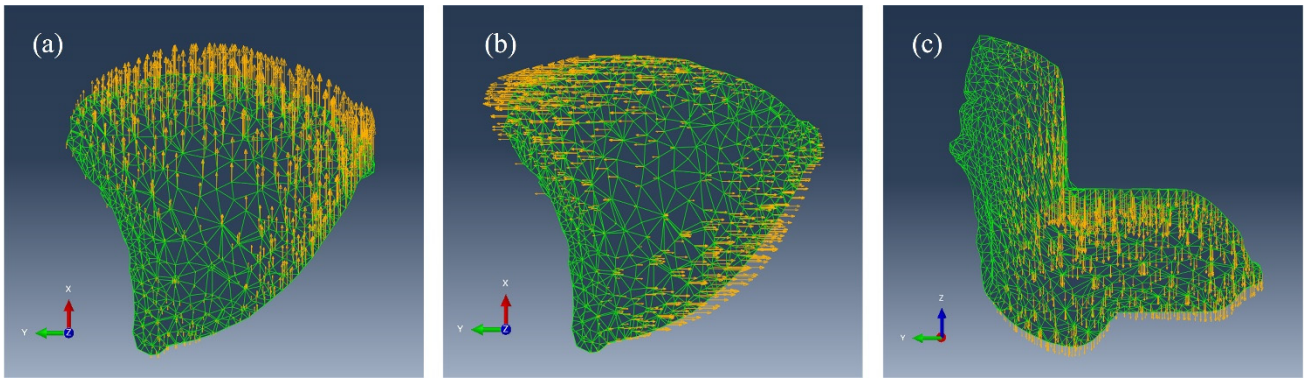

Figure 6. Node displacement of the left breast model: (**a**) medial–lateral direction and (**b**) anterior–posterior direction in the axial plane at 2 cm from the compression paddle, and (**c**) CC direction in the sagittal plane through the nipple. The length of the arrows represents the magnitude of displacement.

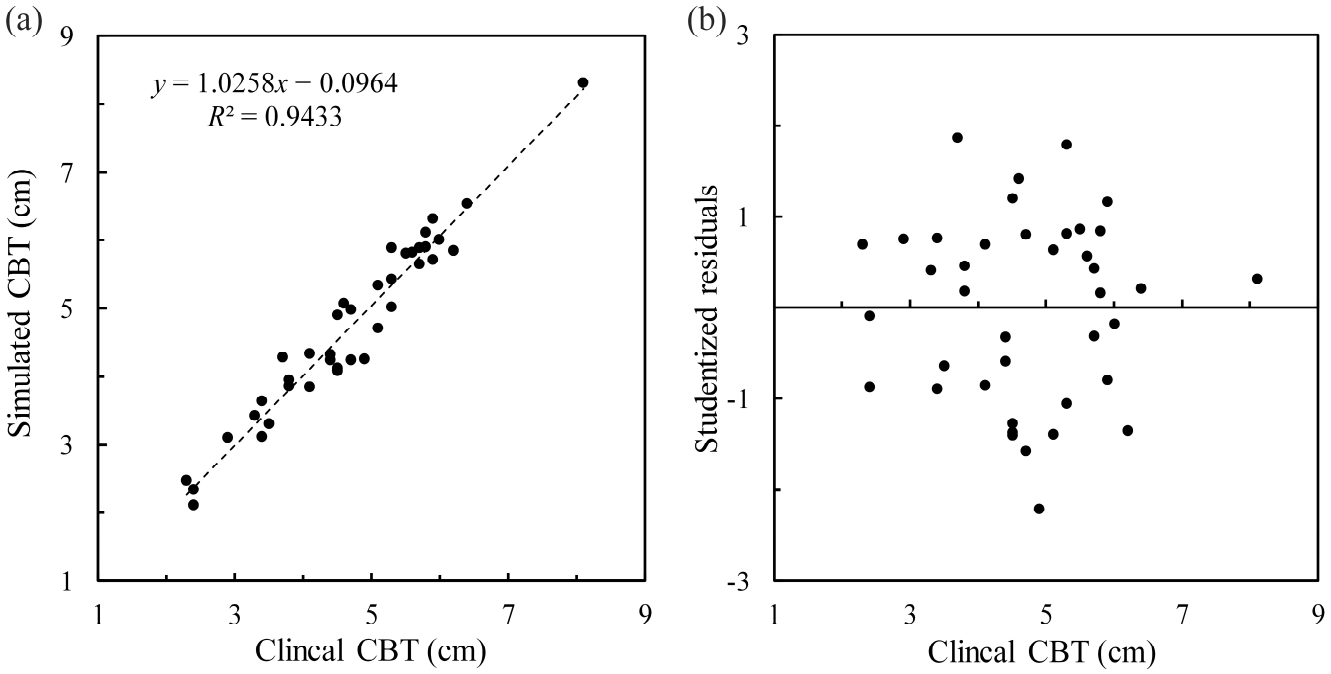

Figure 7. (**a**) Scatter plot of the simulated CBT and the clinical CBT at the same clinical compression force, and (**b**) the studentized residual plot as a function of clinical CBT. The residuals are scattered throughout the clinical CBT without showing any clear trend.

The simulated CBT as a function of breast volume for different compression forces is shown in Figure 8a. The average simulated CBT at 10, 12, 14, and 16 daN was 5.67, 5.13, 4.66, and 4.26 cm, respectively. The simulated CBT was highly positively correlated with breast volume ($r > 0.868$, $p < 0.001$). In Figure 8b, the simulated CBT was plotted against VBD, demonstrating moderate negative correlations at 10, 12, 14, and 16 daN ($r < -0.338$, $p < 0.05$). Combined with the results in Figure 3, once a patient's breast volume or VBD is known through the linear fitting of clinical CBT or directly measuring from MRI or Volpara software [19], we can obtain an appropriate compression force and CBT as clinical recommendations.

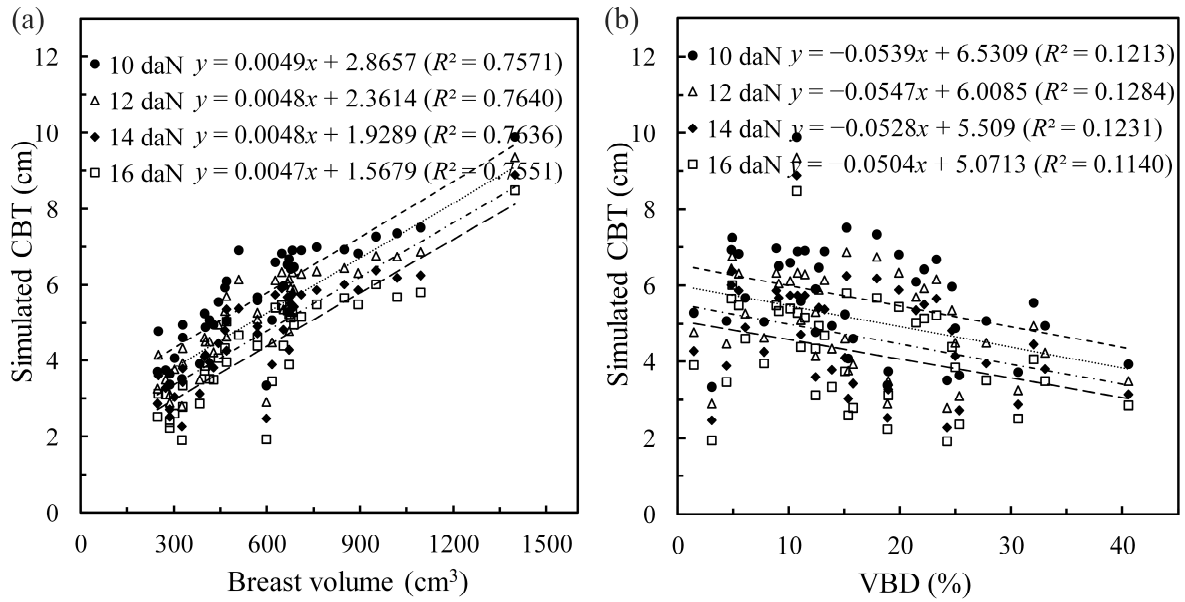

Figure 8. Simulated CBT versus (**a**) breast volume and (**b**) VBD for compression forces of 10, 12, 14, and 16 daN. A strong positive correlation between simulated CBT and breast volume ($r > 0.868$) and a moderate negative correlation between simulated CBT and VBD ($r < -0.338$) are shown.

4. Discussion

The dense breast has more glandular tissue and a higher chance of developing breast cancer [20]. Therefore, several evaluation methods of mammographic parenchymal patterns have been proposed to classify mammographic density, in which the BI-RADS classification divides the breast into four categories, namely extremely dense, heterogeneously dense, scattered, and entirely fatty. Although the BI-RADS category has a strong positive correlation with VBD (Figure 4), it is a qualitative surrogate, and the quantity it represents is not explicit [21]. The correlation between VBD and clinical CBT established in this study (Figure 3b) makes the clinical CBT a potential density indicator for assessing breast cancer risk [22]. High-risk subjects should be mammographically screened at a higher frequency or perform additional breast MRI.

A total of 65 subjects were randomly recruited for this study. The distributions of their CBT, breast volume, and VBD (Figure 2) matched very well with the clinical distributions of Taiwanese women investigated by Dong et al. [18], indicating there is no sampling bias. Such non-uniform sampling does not affect the applicability of the fitting results, while it can provide more accurate compression parameters for most clinical conditions. In other words, the extreme clinical CBT, breast volume, or VBD contribute less to the fitting results and will not significantly affect the suggested compression parameters.

The Mooney-Rivlin model is a kind of hyperelastic model. Although the hyperelastic model has been proven to have more accurate results in breast deformation than the linear model [7], the reliability of the Mooney-Rivlin model in breast compression simulation has not been clinically validated. In this study, the Mooney–Rivlin model was used to perform CBT simulation for different compression forces. The comparison of simulated CBT and clinical CBT shows the accuracy and robustness of the Mooney–Rivlin model, which makes bridging breast MRI and digital mammography possible.

Simulated CBT has a strong positive correlation with breast volume and a moderate negative correlation with VBD. However, other studies have demonstrated a strong negative correlation between CBT and breast density [23,24]. The main reason for this inconsistency is that previous studies used physical tissue-equivalent phantoms, whereas this study used subject-specific breast models. In addition to breast density and volume, the distribution of glandular tissue and breast geometry also affect CBT. Therefore, the correlations we established are more clinically representative.

In clinical practice, a wide variation in the applied compression force is observed in Taiwan. This variation is highly dependent on radiographers and screening sites. The reason for this is that no subject-specific guidelines are currently available for radiographers, who can only rely on their own experience of what suitable compression force is. Based on our findings, a suitable CBT recommendation is provided according to breast volume or VBD information (Figure 3). Then, radiographers can select an optimized compression force to achieve good image quality and avoid patient discomfort (Figure 8). If there are no MR images to obtain breast volume and VBD, we can still use Volpara software or BI-RADS classification to estimate this information [25].

In terms of reducing the discomfort associated with breast compression, recent studies investigated the use of pressure control instead of force control of the compression paddles [26–28]. Although the technique showed the ability to reduce pain, it is a trade-off from thicker CBT. The potential degradation of image quality, mean glandular dose (MGD), and diagnostic performance of mammography is not taken into account during the pressure control procedure. Recently, a large-scale clinical study showed that there were no clinically relevant differences in the pain scores of patients and the compression parameters between the pressure-controlled paddle and the force-controlled paddle [29]. In addition, there was a higher variation of the applied pressure in relation to the breast contact area than the applied compression force [30]. The force-controlled compression technique is still the most used method in the existing mammography and the standard technique recommended by the health care authorities of most countries. Our proposed method is based on the force-controlled compression technique at 10 daN suggested by the mammographic guideline. Patient comfort, image quality, and breast positioning are all taken into account. In addition, this method can be implemented on existing mammography instruments, which is worth promoting in clinical practice.

In addition to providing optimal breast compression parameters, the results of this study can also be applied to breast dosimetry. Currently, MGD, which is the product of the normalized glandular dose (DgN) coefficient and the entrance skin kerma, is widely used for mammography [31]. The DgN coefficient is a function of breast volume, breast density, and CBT. Using the relationships established in this study, once the compression thickness and compression force are known, the breast volume and density can be estimated to index the DgN coefficient and calculate MGD [32]. The incidence of radiation-induced secondary breast malignancy can be further assessed [33].

Women at high risk of breast cancer are often advised to have early mammography and MRI exams, and to increase the frequency of regular breast cancer screening and follow-up with mammography. Through the evidence-based methodology proposed in this study, the tissue information provided by breast MRI can be applied to optimize clinical breast compression parameters for mammography. This allows women to avoid pain and increase compliance with frequent mammography exams while reducing radiation dose to the breast glandular tissue and maintaining the image quality of mammograms.

The limitation of this study is that although the recommended compression force and CBT can be applied to the majority of women, some women may not be able to achieve the recommended parameters due to their particular sensitivity to pain or extreme breast sizes. Radiographers can still refer to the fitting formulas of this study and make appropriate adjustments. In addition, our proposed fitting results may not be suitable for other countries, mainly because of the differences in the distributions of breast volume and density and the breast compression technique used.

5. Conclusions

The relationships between mammographic compression parameters and breast tissue information were established through the construction of subject-specific breast models and the FEM compression simulation. The simulated CBT was highly positively correlated with breast volume and moderately negatively correlated with VBD at 10 to 16 daN. Through this study, a suitable CBT is offered according to breast tissue information. A personalized

and evidence-based compression force suggestion can be provided to radiographers taking into account image quality, patient comfort, and radiation dose.

Author Contributions: Conceptualization, J.W.; methodology, T.-Y.C. and Y.-L.L.; software, H.-C.L.; validation, P.-Y.L. and Y.-L.L.; investigation, P.-Y.L. and Y.-L.L.; resources, T.-Y.C.; data curation, T.-Y.C.; writing—original draft preparation, J.W.; writing—review and editing, J.W., T.-Y.C. and D.L.; visualization, P.-Y.L. and Y.-L.L.; supervision, J.W. All authors have read and agreed to the published version of the manuscript.

Funding: This work was supported by Cheng Hsin General Hospital under the grant number CY10904 and by the Ministry of Science and Technology, Taiwan under the grant number MOST 111-2623-E-A49-002-NU.

Data Availability Statement: The data presented in this study are available on request from the first author.

Acknowledgments: The authors thank Mei Lan Huang from Chi Mei Medical Center, Tainan, Taiwan, for case collection.

Conflicts of Interest: The authors declare no conflict of interest.

References

1. Lehman, C.D.; Wellman, R.D.; Buist, D.S.; Kerlikowske, K.; Tosteson, A.N.; Miglioretti, D.L. Diagnostic accuracy of digital screening mammography with and without computer-aided detection. *Acta Radiol.* **2015**, *175*, 1828–1837. [CrossRef] [PubMed]
2. Suleiman, M.E.; Brennan, P.C.; McEntee, M.F. Diagnostic reference levels in digital mammography: A systematic review. *Radiat. Prot. Dosim.* **2015**, *167*, 608–619. [CrossRef] [PubMed]
3. Moshina, N.; Sagstad, S.; Sebuødegård, S.; Waade, G.G.; Gran, E.; Music, J.; Hofvind, S. Breast compression and reported pain during mammographic screening. *Radiography* **2020**, *26*, 133–139. [CrossRef] [PubMed]
4. Dong, S.L.; Chu, T.C.; Lin, Y.C.; Lan, G.Y.; Yeh, Y.H.; Chen, S.; Chuang, K.S. Determination of equivalent breast phantoms for different age groups of Taiwanese women: An experimental approach. *Med. Phys.* **2011**, *38*, 4094–4100. [CrossRef]
5. Partovi, S.; Sin, D.; Lu, Z.; Sieck, L.; Marshall, H.; Pham, R.; Plecha, D. Fast MRI breast cancer screening—Ready for prime time. *Clin. Imaging* **2020**, *60*, 160–168. [CrossRef]
6. Esslinger, D.; Rapp, P.; Knödler, L.; Preibsch, H.; Tarín, C.; Sawodny, O.; Brucker, S.Y.; Hahn, M. A novel finite element model-based navigation system-supported workflow for breast tumor excision. *Med. Biol. Eng. Comput.* **2019**, *57*, 1537–1552. [CrossRef]
7. Garcia, E.; Diez, Y.; Diaz, O.; Llado, X.; Marti, R.; Marti, J.; Oliver, A. A step-by-step review on patient-specific biomechanical finite element models for breast MRI to x-ray mammography registration. *Med. Phys.* **2018**, *45*, e6–e31. [CrossRef]
8. Shih, T.C.; Chen, J.H.; Liu, D.; Nie, K.; Sun, L.; Lin, M.; Chang, D.; Nalcioglu, O.; Su, M.Y. Computational simulation of breast compression based on segmented breast and fibroglandular tissues on magnetic resonance images. *Phys. Med. Biol.* **2010**, *55*, 4153–4168. [CrossRef]
9. Thanoon, D.; Garbey, M.; Bass, B.L. Deriving indicators for breast conserving surgery using finite element analysis. *Comput. Methods Biomech. Biomed. Eng.* **2015**, *18*, 533–544. [CrossRef]
10. Pianigiani, S.; Ruggiero, L.; Innocenti, B. An anthropometric-based subject-specific finite element model of the human breast for predicting large deformations. *Front. Bioeng. Biotechnol.* **2015**, *3*, 201. [CrossRef]
11. Lapuebla-Ferri, A.; Cegonino-Banzo, J.; Jimenez-Mocholi, A.J.; Del Palomar, A.P. Towards an in-plane methodology to track breast lesions using mammograms and patient-specific finite-element simulations. *Phys. Med. Biol.* **2017**, *62*, 8720–8738. [CrossRef] [PubMed]
12. Green, C.A.; Goodsitt, M.M.; Brock, K.K.; Davis, C.L.; Larson, E.D.; Lau, J.H.; Carson, P.L. Deformable mapping technique to correlate lesions in digital breast tomosynthesis and automated breast ultrasound images. *Med. Phys.* **2018**, *45*, 4402–4417. [CrossRef] [PubMed]
13. Ismail, H.M.; Pretty, C.G.; Signal, M.K.; Haggers, M.; Chase, J.G. Finite element modelling and validation for breast cancer detection using digital image elasto-tomography. *Med. Biol. Eng. Comput.* **2018**, *56*, 1715–1729. [CrossRef] [PubMed]
14. Mehrabian, H.; Richmond, L.; Lu, Y.; Martel, A.L. Deformable registration for longitudinal breast MRI screening. *J. Digit. Imaging* **2018**, *31*, 718–726. [CrossRef]
15. Waade, G.G.; Moshina, N.; Sebuodegard, S.; Hogg, P.; Hofvind, S. Compression forces used in the Norwegian Breast Cancer Screening Program. *Br. J. Radiol.* **2017**, *90*, 20160770. [CrossRef]
16. Rao, A.A.; Feneis, J.; Lalonde, C.; Ojeda-Fournier, H. A pictorial review of changes in the BI-RADS Fifth Edition. *Radiographics* **2016**, *36*, 623–639. [CrossRef]
17. Yin, H.M.; Sun, L.Z.; Wang, G.; Yamada, T.; Wang, J.; Vannier, M.W. ImageParser: A tool for finite element generation from three-dimensional medical images. *Biomed. Eng. Online* **2004**, *3*, 31. [CrossRef]
18. Dong, S.L.; Chu, T.C.; Lan, G.Y.; Lin, Y.C.; Yeh, Y.H.; Chuang, K.S. Development of an adjustable model breast for mammographic dosimetry assessment in Taiwanese women. *AJR Am. J. Roentgenol.* **2011**, *196*, W476–W481. [CrossRef]

19. Fedon, C.; Caballo, M.; García, E.; Diaz, O.; Boone, J.M.; Dance, D.R.; Sechopoulos, I. Fibroglandular tissue distribution in the breast during mammography and tomosynthesis based on breast CT data: A patient-based characterization of the breast parenchyma. *Med. Phys.* **2021**, *48*, 1436–1447. [CrossRef]
20. Wanders, J.O.P.; van Gils, C.H.; Karssemeijer, N.; Holland, K.; Kallenberg, M.; Peeters, P.H.M.; Nielsen, M.; Lillholm, M. The combined effect of mammographic texture and density on breast cancer risk: A cohort study. *Breast Cancer Res.* **2018**, *20*, 36. [CrossRef]
21. Sartor, H.; Lang, K.; Rosso, A.; Borgquist, S.; Zackrisson, S.; Timberg, P. Measuring mammographic density: Comparing a fully automated volumetric assessment versus European radiologists' qualitative classification. *Eur. Radiol.* **2016**, *26*, 4354–4360. [CrossRef] [PubMed]
22. McCormack, V.A.; dos Santos Silva, I. Breast density and parenchymal patterns as markers of breast cancer risk: A meta-analysis. *Cancer Epidemiol. Biomark. Prev.* **2006**, *15*, 1159–1169. [CrossRef] [PubMed]
23. Geise, R.A.; Palchevsky, A. Composition of mammographic phantom materials. *Radiology* **1996**, *198*, 347–350. [CrossRef] [PubMed]
24. Jamal, N.; Ng, K.H.; McLean, D.; Looi, L.M.; Moosa, F. Mammographic breast glandularity in Malaysian women: Data derived from radiography. *AJR Am. J. Roentgenol.* **2004**, *182*, 713–717. [CrossRef] [PubMed]
25. Lee, H.N.; Sohn, Y.M.; Han, K.H. Comparison of mammographic density estimation by Volpara software with radiologists' visual assessment: Analysis of clinical-radiologic factors affecting discrepancy between them. *Acta Radiol.* **2015**, *56*, 1061–1068. [CrossRef]
26. de Groot, J.E.; Branderhorst, W.; Grimbergen, C.A.; den Heeten, G.J.; Broeders, M.J.M. Towards personalized compression in mammography: A comparison study between pressure-and force-standardization. *Eur. J. Radiol.* **2015**, *84*, 384–391. [CrossRef] [PubMed]
27. de Groot, J.E.; Hopman, I.G.M.; van Lier, M.; Branderhorst, W.; Grimbergen, C.A.; den Heeten, G.J. Pressure-standardised mammography does not affect visibility, contrast and sharpness of stable lesions. *Eur. J. Radiol.* **2017**, *86*, 289–295. [CrossRef]
28. Moshina, N.; Larsen, M.; Holen, Å.S.; Waade, G.G.; Aase, H.S.; Hofvind, S. Digital breast tomosynthesis in a population based mammographic screening program: Breast compression and early performance measures. *Eur. J. Radiol.* **2021**, *139*, 109665. [CrossRef]
29. Jeukens, C.; van Dijk, T.; Berben, C.; Wildberger, J.E.; Lobbes, M.B.I. Evaluation of pressure-controlled mammography compression paddles with respect to force-controlled compression paddles in clinical practice. *Eur. Radiol.* **2019**, *29*, 2545–2552. [CrossRef]
30. Serwan, E.; Matthews, D.; Davies, J.; Chau, M. Mechanical standardisation of mammographic compression using Volpara software. *Radiography* **2021**, *27*, 789–794. [CrossRef]
31. Boone, J.M. Normalized glandular dose (DgN) coefficients for arbitrary X-ray spectra in mammography: Computer-fit values of Monte Carlo derived data. *Med. Phys.* **2002**, *29*, 869–875. [CrossRef] [PubMed]
32. Chang, T.Y.; Lai, K.J.; Tu, C.Y.; Wu, J. Three-layer heterogeneous mammographic phantoms for Monte Carlo simulation of normalized glandular dose coefficients in mammography. *Sci. Rep.* **2020**, *10*, 2234. [CrossRef] [PubMed]
33. NRC. *Health Risks from Exposure to Low Levels of Ionizing Radiation: BEIR VII Phase 2*; National Academies Press: Washington, DC, USA, 2006; Volume 7.